INFLUENCE OF LOCAL ATOMIC AND ELECTRONIC STRUCTURES OF MAGNETITE ON SUBTLE EFFECTS IN HERFD-XANES SPECTRA

Yu. S. Podkovyrina, M. A. Kremennaya,
M. A. Soldatov, and A. V. Soldatov

Large iron oxide nanoparticles are studied by high-energy resolution fluorescence-detected X-ray absorption spectroscopy (HERFD XANES). A theoretical procedure within the finite-difference method framework is tested to calculate Fe K-edge X-ray absorption spectra for the magnetite structure. The influence of structural and non-structural calculation parameters on the subtle effects in the X-ray absorption spectra are considered. Tetrahedral positions of Fe^{3+} ions are shown to provide the main contribution to the spectral feature at 20-21 eV whose intensity grows together with the content of these ions.

INTRODUCTION

The continuing interest in iron oxide magnetic nanoparticles (MNPs) is primarily due to their unique properties to be used in biomedicine [1-3]. One of the most important applications is local hyperthermia [4-6] which is used to overheat and neutralize unwanted tissues in the body, in particular, deep-seated cancer tumors. The properties of iron oxide MNPs can be used to prepare contrast agents for NMR tissue imaging [7, 8]. Detailed understanding of physical and chemical properties of MNPs provides possibilities to obtain MNPs with required parameters [9].

Maghemite (γ-Fe_2O_3) and magnetite (Fe_3O_4) are distinguished among other magnetic phases of iron oxides due to strong magnetic moments and some features of their local atomic and electronic structures. Unlike other magnetic phases, magnetite contains both Fe^{2+} and Fe^{3+} ions. Magnetite Fe_3O_4 displays the inverse spinel structure, with half of Fe^{3+} ions appearing in tetrahedral positions and Fe^{3+} and Fe^{2+} distributed equally over octahedral positions. Despite the fact that the magnetite structure has been known for more than a hundred years [10], new details of its electronic structure in macrocrystalline samples are still discovered [11]. In contrast to magnetite, maghemite contains only Fe^{3+} ions. It also displays the inverse spinel structure along with structural vacancies, whose distribution is of undoubted interest [12]. The structural details of iron oxide MNPs are still broadly discussed [13].

Fe K-edge XANES (X-ray Absorption Near Edge Structure) spectra are sensitive both to the charge state of the absorbing atom and to its three-dimensional local environment [14-16]. For example, there is a chemical shift of the absorption edge by more than 3 eV in the spectra of compounds containing Fe^{3+} and Fe^{2+} [17]. It was also shown that the ratio Fe^{3+}/Fe^{total} can be estimated using XANES spectroscopy with an accuracy comparable to that of Mossbauer spectroscopy [18]. The advantage of measuring Fe K-edge XANES spectra rather than $L_{2,3}$-edge spectra is due to the sensitiveness of the former to slight changes in interatomic distances and bond angles near the absorbing atom, while $L_{2,3}$ spectra are sensitive to the point symmetry of the position of the absorbing atom [13].

Theoretical simulations of K-edge absorption XANES spectra can be used to expand the possibilities of experimental methods. A precise description of experimental Fe K-edge X-ray absorption spectra requires that non-structural calculation parameters are to be chosen and fixed. The calculated spectra are used to understand the features of MNP structure as compared to macrocrystalline samples.
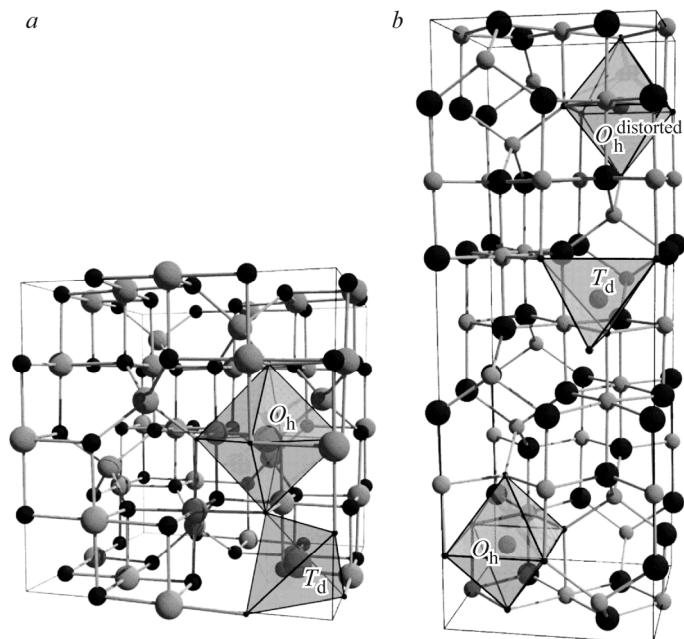
EXPERIMENTAL

The experimental Fe K-edge HERFD-XANES (High-Energy Resolution Fluorescence-Detected XANES) in magnetite (Sigma Aldrich 518158) was recorded on a ID26 station [19] of the European synchrotron radiation facility (ESRF) (Grenoble, France). The schematic experimental setup is shown in Fig. 1. The Fe K-edge excitation energy was set up using two liquid monochromator crystals Si (311) cooled by liquid nitrogen. Higher harmonics were suppressed using three silicon mirrors operating in the full-field reflection mode. Metallic iron foil was used to calibrate the monochromator energy. The emission spectrometer was equipped with four spherically bent crystals Ge(440) arranged with the sample and an avalanche photodiode in the vertical Roland geometry ($R = 1$ m) at an angle of 90° with respect to the scattering angle. The analyzer crystals were masked to improve the resolution. The total experimental broadening defined as the average arithmetic half-width of the elastic profiles was about 0.5 eV. The Fe K-edge HERFD-XANES spectrum was recorded by scanning the energy of incident photons, the emission monochromator was fixed at the maximum energy of Fe$K\alpha_1$ emission line. The measurements were carried out at 20 K to minimize the radiation damage.

THEORETICAL

Theoretical calculations of Fe K-edge XANES spectra in magnetite were performed using the FDMNES package (Finite Difference Method for Near Edge Structure) [20]. FDMNES includes two calculation procedures: the finite-difference method and the method of complete multiple scattering. The first method implies the finite-difference approach to solve the Schrödinger equation in a spherical region around the absorbing atom. Both the *muffin-tin* approximation and the full potential approximation were tested without any restrictions imposed on its form. The solution of the Schrödinger equation was searched over a grid of points in a spherical region encompassing the absorbing atom and extending over a sufficiently large cluster [20]. The second method implies Green's formalism and is restricted by the *muffin-tin* potential approximation. Two structural models of Fe_3O_4 were used for the calculation: the cubic structure Fd-3m (Fig. 2a) [21] and the monoclinic
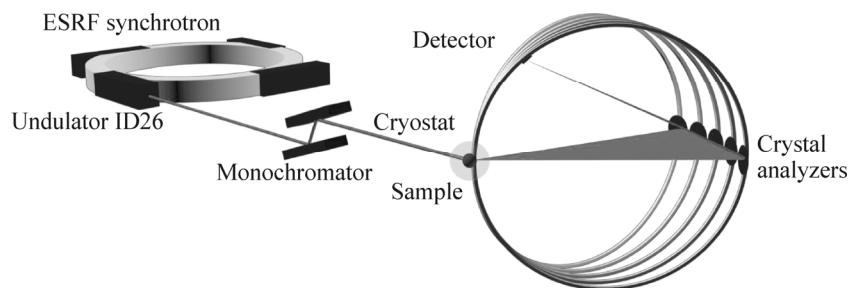
Fig. 1. Schematic setup ID26 to record HERFD-XANES spectra.

Fig. 2. Cubic (*a*) and monoclinic (*b*) unit cells for the Fe_3O_4 structure.

structure $P2/c$ (Fig. 2*b*) [22]. The cluster was 5 Å in size with 56 atoms in the first case, and 5 Å with 51 atoms in the second case. The similarity between theoretical and experimental spectra was estimated as:

$$R_f = \sum_e ((E(e) - T(e))^2)/\sum_e ((E(e))^2),$$

where $\sum_e$ is the sum over energies; $E(e)$ are experimental intensities; $T(e)$ are calculated intensities.

RESULTS AND DISCUSSION

Magnetite at room temperature displays a cubic Fd-$3m$ structure with the cell parameter $a = 8.394$ Å. There are two nonequivalent positions of Fe in this magnetite structure. The iron ion appears in the tetrahedral (T_d) environment of oxygen atoms in the first case and in a slightly distorted octahedral (O_h) environment in the second case. According to ionic description, the charge of iron is 2.5+ in the octahedral position and 3+ in the tetrahedral position. The Verwey transition reduces the symmetry of the unit cell to $P2/c$ monoclinic symmetry (Fig. 2*b*) with numerous nonequivalent positions [22].

The Fe K-edge XANES spectrum in magnetite is formed by superposing the spectra calculated for all non-equivalent positions with corresponding weights. As mentioned above, the cubic structure of magnetite is characterized by T_d and O_h non-equivalent positions appearing in a 1:2 ratio, respectively (Fig. 3*a*).

The above XANES spectra were calculated for tetrahedral and octahedral non-equivalent positions using the finite-difference method in the full potential approximation. The quadrupole approximation for selection rules displayed no significant spectral changes (except for a slight change in the intensity of the pre-edge structure *a*). Therefore, we discuss here the spectra calculated within the dipole approximation. The spectrum calculated for the nonequivalent O_h position demonstrates higher intensities of the main maximum *c* and peak *d* compared to the T_d position. On the other hand, the T_d spectra demonstrate a higher shoulder *b* on the absorption edge at 4-5 eV, while the main maximum *c* and peak *e* shift to the high-energy region. The weighted composition of the spectra calculated for non-equivalent positions T_d and O_h exhibits the form characteristic of O_h with noticeably increased intensity of the feature *b*, while the main maximum *c* and peak *e* are shifted to the high-energy region. Fig. 3*b* compares the spectra calculated by the finite-difference method and the method of
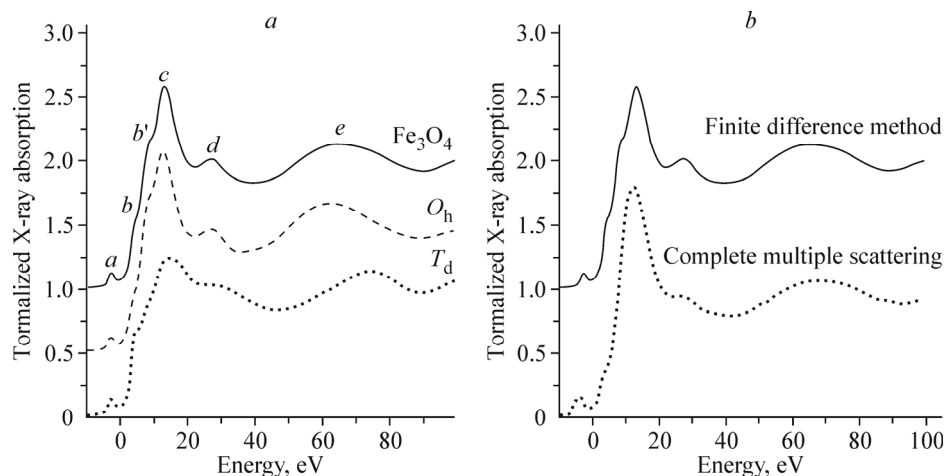
Fig. 3. Spectra calculated for non-equivalent T_d (dotted line) and O_h (dashed line), and the spectrum for the magnetite cubic structure (solid line) as a result of superposing the above spectra in a ratio of 1:2, respectively (*a*); theoretical spectra calculated by the finite difference method (solid line) and the method of complete multiple scattering (dotted line) (*b*).

complete multiple scattering with a self-consistent potential to demonstrate a higher intensity of the main maximum and less pronounced features of *b* and *b'*.

The XANES spectra for the monoclinic structure reported in this work were also calculated for all nonequivalent positions using the finite-difference method in the full-potential approximation. In this case, there are nine such positions: 5 positions with the iron ion coordinated by six oxygen atoms in a close-to-octahedral environment, 3 positions with the iron ion coordinated by four oxygen atoms in a close-to-tetrahedral environment, and 1 position with the iron ion coordinated by six oxygen atoms in a strongly distorted octahedral environment $O_h^{distorted}$ (Fig. 4*a*). The shape of the spectra for
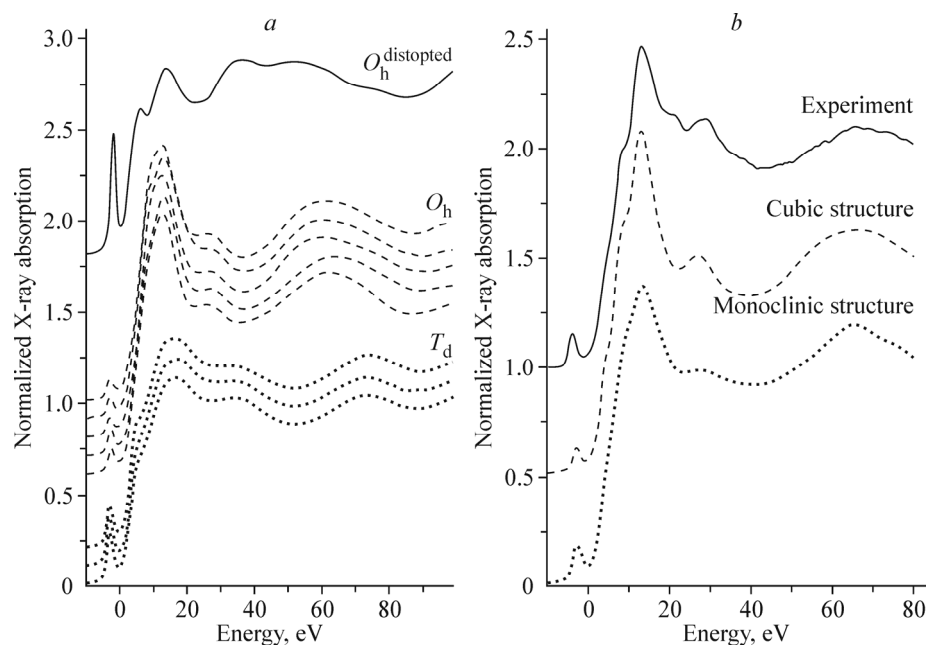
Fig. 4. Spectra calculated for several series of nonequivalent positions T_d (dotted line), O_h (dashed line), and distorted octahedron $O_h^{distorted}$ (solid line) (*a*); experimental spectrum (solid line) and spectra calculated for the cubic (dashed line) and monoclinic structures (dotted line) by the finite difference method (*b*).

nonequivalent positions T_d and O_h is similar to that of nonequivalent positions for the cubic structure. The only exception is the $O_h^{distorted}$ position. However, the specific weight of this spectrum slightly exceeds 6 percent, which is not a significant contribution to the shape of the resulting spectrum.

Various electronic configurations of atomic orbitals were tested for these structures. However, this did not improve the agreement between theoretical and experimental spectra. Two calculations were performed to test the effect of the electronic structure: the one with partial charge transfer $Fe^{2.5+}$ ($3d^{5.5}$), and the one with full charge transfer Fe^{3+} and Fe^{2+} ($3d^5$ and $3d^6$, respectively). These parameters were found to broaden the spectral features without improving the agreement between theoretical and experimental spectra. A numerical comparison of theoretical Fe K-edge XANES spectra with the experimental spectra in the cubic and monoclinic magnetite phases (Fig. 4b) shows that the spectrum calculated for the monoclinic structure is in better agreement with the experimental spectrum ($R_f = 0.038$) than the spectrum calculated for the cubic structure ($R_f = 0.054$).

CONCLUSIONS

The parameters of theoretical simulation of Fe K-edge XANES X-ray absorption spectra were tested for cubic and monoclinic structures to consider the influence of various non-structural calculation parameters such as the choice of the calculation method (finite-difference method or the method of multiple scattering), the account of the self-consistent potential, quadrupole effects, and electronic configuration of Fe ions in non-equivalent positions. It was shown that the best agreement between calculated and experimental spectra is achieved for the monoclinic structure, and varying the above parameters does not significantly improve the agreement in the case of the cubic structure. The main maximum in the theoretical spectrum of the Fe ion in the tetrahedral position shifts towards higher energies, which can cause the experimental feature observed at 20-21 eV. Thus, the increased intensity of this feature can be explained by increased concentration of tetrahedral positions in the structure of magnetite samples.

REFERENCES

1. S. Laurent, D. Forge, M. Port, A. Roch, C. Robic, L. Vander Elst, and R. N. Muller. *Chem. Rev.*, **2008**, *108*, 2064-2110.
2. Q. A. Pankhurst, N. T. K. Thanh, S. K. Jones, and J. Dobson. *J. Phys. D: Appl. Phys.*, **2009**, *42*, 224001.
3. T. Pedro, M. María del Puerto, V.-V. Sabino, G.-C. Teresita, and J. S. Carlos. *J. Phys. D: Appl. Phys.*, **2003**, *36*, R182.
4. A. E. Deatsch and B. A. Evans. *J. Magn. Magn. Mater.*, **2014**, *354*, 163-172.
5. P. Drake, H.-J. Cho, P.-S. Shih, C.-H. Kao, K.-F. Lee, C.-H. Kuo, X.-Z. Lin, and Y.-J. Lin. *J. Mater. Chem.*, **2007**, *17*, 4914.
6. Y. Lv, Y. Yang, J. Fang, H. Zhang, E. Peng, X. Liu, W. Xiao, and J. Ding. *Rsc Adv.*, **2015**, *5*, 76764-76771.
7. J. F. Berret, N. Schonbeck, F. Gazeau, D. El Kharrat, O. Sandre, A. Vacher, and M. Airiau. *J. Am. Chem. Soc.*, **2006**, *128*, 1755-1761.
8. R. Hachani, M. Lowdell, M. Birchall, A. Hervault, D. Mertz, S. Begin-Colin, and N. T. Thanh. *Nanoscale*, **2016**, *8*, 3278-87.
9. M. Levy, A. Quarta, A. Espinosa, A. Figuerola, C. Wilhelm, M. García-Hernández, A. Genovese, A. Falqui, D. Alloyeau, R. Buonsanti, P. D. Cozzoli, M. A. García, F. Gazeau, and T. Pellegrino. *Chem. Mater.*, **2011**, *23*, 4170-4180.
10. W. H. Bragg. *Nature*, **1915**, *95*, 561.

11. M. S. Senn, J. P. Wright, and J. P. Attfield. *Nature*, **2012**, *481*, 173-176.

12. A. V. Korobeinikova, V. I. Fadeeva, and L. A. Reznitskii. *J. Struct. Chem.*, **1976**, *17*, 737-741.

13. C. Piquer, M. A. Laguna-Marco, A. G. Roca, R. Boada, C. Guglieri, and J. Chaboy. *J. Phys. Chem. C*, **2014**, *118*, 1332-1346.

14. J. A. van Bokhoven and C. Lamberti. X-Ray Absorption and X-Ray Emission Spectroscopy: Theory and Applications. Chichester: Wiley, **2016**.

15. A. Bianconi, M. Dell′Ariccia, A. Gargano, and C. R. Natoli. EXAFS and Near Edge Structure. Berlin: Springer-Verlag, **1983**.

16. O. E. Polozhentsev, S. P. Kubrin, V. V. Butova, V. K. Kochkina, A. V. Soldatov, and V. V. Stashenko. *J. Struct. Chem.*, **2016**, *57*, 1459-1468.

17. H. Okudera, A. Yoshiasa, K.-i. Murai, M. Okube, T. Takeda, and S. Kikkawa. *J. Mineral. Petrol. Sci.*, **2012**, *107*, 127-132.

18. A. J. Berry, G. M. Yaxley, A. B. Woodland, and G. J. Foran. *Chem. Geology*, **2010**, *278*, 31-37.

19. P. Glatzel and A. Juhin. In: X-ray Absorption and Emission Spectroscopy" in Local Structural Characterisation / Eds. D. W. Bruce, D. O′Hare and R. I. Walton. UK, Chichester: John Wiley & Sons, **2013**, 89-171.

20. Y. Joly. *Phys. Rev. B*, **2001**, *63*, 125120.

21. C. Haavik, S. Stølen, H. Fjellvåg, M. Hanfland, and D. Häusermann. *Am. Mineral.*, **2000**, *85*, 514-523.

22. Y. Joly, O. Bunău, J. E. Lorenzo, R. M. Galéra, S. Grenier, and B. Thompson. *J. Phys.: Conf. Ser.*, **2009**, *190*, 012007.